Performance of a Behavioural Model with Long-Term Memory Effects

Carlos Crespo-Cadenas[1], Javier Reina-Tosina[1], María J. Madero-Ayora[1]

[1] University of Seville, Dept. of Signal Theory and Communications, Escuela Técnica Superior de Ingeniería, Camino de los Descubrimientos s/n, Seville, 41092, Spain

This paper presents a new behavioural model for power amplifiers that accomplishes the capture of nonlinear low-frequency memory effects with a reduced complexity and a superior precision. It has been extensively evaluated with a commercial amplifier using WCDMA-like modulated data with symbol rates in the range of 2 ksym/s to 1 Msym/s, and it is shown that the first dynamic reduction of the proposed model is successfully compared with other highly efficient methods in terms of complexity and generalization capacity.

Corresponding author: C. Crespo-Cadenas; email: ccrespo@us.es; phone: +34 954487336

I. INTRODUCTION

The role of non-linear impairments in wireless communications systems is currently focusing the interest of researchers in order to bridge the gap of the efficiency-versus-linearity trade-off, together with the benefits that can be derived from novel hardware and software architectures for compensating the nonlinear behaviour, either at the transmitter or the receiver sides. The synergistic interaction of the increasing computing and simulation power with nonlinear measurement instrumentation has pushed the interest of behavioural modelling (BM) applied to wireless design at system level, being the power amplifier (PA) the most critical subsystem.

Several BM approaches have been successfully developed to characterize nonlinear memory effects in PAs [1]. Among the class of Volterra-based behavioural models, in addition to the Memory Polynomial (MP) model, excellent performance has been accomplished by the Generalized Memory Polynomial (GMP) [2] and Dynamic Deviation Reduction (DDR) [3–4] models. The structure of the GMP model involves envelope waveforms with different time shifts, embodying the so-called cross-terms. In the DDR representation, the terms of the full-Volterra (FV) structure are reorganized depending on the order of dynamics involved in the model. Thus, each Volterra kernel is classified according to its corresponding nonlinearity and dynamic order, and the reduction in the model complexity is also attained by controlling the value of this dynamic order.

While most of the BM proposals follow a heuristic reasoning, the use of specific physical knowledge has enabled a deeper understanding of the model structure and its connection with the PA equivalent circuit [5] or the device physical properties [6]. An example is the inclusion of the physical phenomenon of self-heating by considering the contribution of thermal power feedback (TPF). In [7], the authors applied TPF to the equivalent circuit of a unilateral FET device to derive a continuous time representation of the PA response in presence of long-term memory effects. The resulting model enabled the reliable prediction of the dynamics of pulsed RF waveforms with two PAs and the dependence of AM/AM and AM/PM characteristics with symbol rate. In [8], a similar approach led to the formal derivation of a third-order discrete-time BM. Its structure could be represented in terms of a bank of parallel filters driven by the instantaneous power, with each filter tuned at a different frequency sub-band in order to provide a reliable representation of memory effects in a wide range of signal bandwidths.

The objective of this paper is to generalize the model structures presented in [7–8] and derive a novel baseband BM that can be favourably tested against other popular models. A discrete-time representation of the model presented in [7] is derived in Section II, by applying conventional nonlinear circuit analysis to demonstrate the kernel constitution. Particularization to the common scenario of RF signals, covering narrow bandwidths with respect to the generally flat amplifier response, is shown to enable further reduction in the model complexity. While the third-order kernel exhibits the same structure than that of [8], the expressions are generalized for higher orders and the terms are rearranged regarding the order of filtering, what allows the representation of nonlinear memory effects in increasing dynamic orders. Section III presents a discussion of the resulting behavioural model and it is compared with other well-established approaches in terms of complexity. Section IV is dedicated to test the performance of this technique with experimental data using time and spectral domain measurements. Finally, Section V presents some concluding remarks.

II. DERIVATION OF THE DISCRETE-TIME BASEBAND MODEL

According to [7], a simple structure that enables the consideration of long-term memory effects is the simplified unilateral equivalent circuit of a FET device with a feedback path coupling the nonlinear currents to a “thermal” node. Voltages at the gate-to-source capacitor, thermal and output nodes will be denoted as $v(t)$, $\theta(t)$ and $y(t)$, respectively. We will consider well-designed impedance matching networks, memoryless at the input and with a bandpass response centred at the carrier frequency at the output. The drain current is expanded in Taylor series as:

$$i(v,\theta)=\sum_{\mu=1}^{\infty} g_{\mu} v^{\mu} + \sum_{\mu,\upsilon=1}^{\infty} \gamma_{\mu\nu} v^{\mu}\theta^{\nu} + \sum_{\nu=1}^{\infty} \gamma_{0\nu}\theta^{\nu} \tag{1}$$

where μ, ν are discrete summation indices. As stated by the approach demonstrated in [5], the first step is to deduce the nth-order nonlinear transfer functions $H_{gn}(\omega_1, \ldots, \omega_n)$ and $H_n(\omega_1, \ldots, \omega_n)$, relating the complex envelopes $v(t)$ and $y(t)$ with the input waveform, respectively.

In this case, it is also necessary to consider the thermal transfer functions $H_{\theta n}(\omega_1, \ldots, \omega_n)$ relating the temperature rise $\theta(t)$ with the input. After the results published in [9], we can deduce that $H_{gn}(\omega_1, \ldots, \omega_n) = 0$ for $n \geq 2$, and that there is no linear relation between $\theta(t)$ and the input voltage. Since $H_{\theta 1}(\omega) = 0$, the linear output transfer function is $H_1(\omega) = -g_1 H_{g1} Z_0(\omega)$, where $Z_0(\omega)$ is the output impedance.

Considering that the thermal response presents a lowpass characteristic, self-heating can be related to the low-frequency components of the nonlinear current [8]. Therefore, the second-order thermal transfer function can be written as

$$H_{\theta 2}(\omega_1, \omega_2) = -g_2 |H_{g1}|^2 Z_\theta(\omega_1 + \omega_2), \tag{2}$$

where $Z_\theta(\omega)$ is the thermal impedance connecting the thermal-node to ground, modelled as an RC low-pass filter. Observe that (2) is a lowpass function dependent on $\omega_1+\omega_2$, negligible outside the baseband zone.

Following a similar analysis to that contained in [9], it can be observed that the third-order nonlinear current presents components at the fundamental frequency and the third harmonic bands. Since no electro-thermal path interconnecting the drain and the thermal-node exists in these bands, no low-frequency dispersive terms are produced, and $H_{\theta 3}(\omega_1, \omega_2, \omega_3) = 0$. The third-order transfer function for the output was deduced in [8]:

$$\begin{aligned} H_3(\omega_1, \omega_2, \omega_3) = -[\, & g_3 |H_{g1}|^2 H_{g1} Z_0(\omega_1+\omega_2+\omega_3) + \\ & + \gamma_{11} \overline{H_{g1}(\omega_1) H_{\theta 2}(\omega_2, \omega_3)} Z_0(\omega_1 + \omega_2 + \omega_3) \,] \end{aligned} \tag{3}$$

inside the fundamental zone, and zero otherwise. The overbar indicates symmetrization of the Volterra transfer function product. The first term in (3) is memoryless, but the second one takes into account the connection of the drain current and the temperature rise, $\theta(t)$, through the electro-thermal path, and is the responsible for the low-frequency dispersive effects. Once the nonlinear transfer function (3) is known, and relying on the assumption that the input signal is band-limited, the corresponding third-order component of the discrete-time complex envelope can be derived by following the procedure described in [5], and is expressed as

$$y_3(k) = h_{30} |x(k)|^2 x(k) + \sum_{q_1=0}^{Q} \sum_{q_2=1}^{Q} h_{31}^{(\theta)}(q_1, q_2) |x(k - q_2 - q_1)|^2 x(k - q_1) \tag{4}$$

where k is the discrete time index and Q stands for the memory length. The memoryless term includes both electrical and thermal effects, and the sum represents the dynamic deviation induced by the thermal effects.

In a similar fashion, the fifth-order term can be expressed as

$$\begin{aligned} y_5(k) = {} & h_{50} |x(k)|^4 x(k) + \sum_{q_1=0}^{Q} \sum_{q_2=1}^{Q} h_{51}^{(\theta)}(q_1, q_2) |x(k - q_2 - q_1)|^2 |x(k - q_1)|^2 x(k - q_1) + \\ & + \sum_{q_1=0}^{Q} \sum_{q_2=1}^{Q} \sum_{q_3=1}^{Q} h_{52}^{(\theta)}(q_1, q_2, q_3) |x(k - q_2 - q_1)|^2 |x(k - q_3 - q_1)|^2 x(k - q_1) + \ldots . \end{aligned} \tag{5}$$

Here, the first term represents the static part, electrical and thermal. The dynamic part, generated by the electro-thermal filter, is composed by two terms with sums on the discrete delays. An additional simplification can be included by assuming a flat response for the output impedance in the signal bandwidth [5], i.e. $q_1 = 0$ in the summations of (4) and (5). In this form, $y_5(k)$ is described by a first term, memoryless, a second term with a linear convolution, and a third term with a two-dimensional convolution. The same procedure to gather the sums can be extended to higher-order terms of $y(k)$, allowing a final representation with the elements collected regarding the order of filtering. This form of grouping the coefficients makes possible to express the output of the PA separated into a memoryless and a dynamic part, as follows

$$y(k) = y_0(k) + y_d(k), \tag{6}$$

where $y_0(k)$ is given by

$$y_0(k) = [\, h_{10} + h_{30}|x(k)|^2 + h_{50}|x(k)|^4 + \\ + h_{70}|x(k)|^6 + \ldots +]\, x(k)\,. \tag{7}$$

The dynamic characteristic can be separated in compliance with the aforementioned order of filtering, $y_d(k) = y_{d1}(k) + y_{d2}(k) + \ldots$. The first dynamic component, associated to linear filtering, can be written as

$$y_{d1}(k) = \sum_{q=1}^{Q} [h_{31}^{(\theta)}(q) + h_{51}^{(\theta)}(q)|x(k)|^2 + \\ + h_{71}^{(\theta)}(q)|x(k)|^4 + \cdots]|x(k-q)|^2 x(k)\ , \tag{8}$$

the second dynamic component entails quadratic filtering, expressed as

$$y_{d2}(k) = \sum_{q_1=1}^{Q}\sum_{q_2=1}^{Q} [h_{52}^{(\theta)}(q_1,q_2) + h_{72}^{(\theta)}(q_1,q_2)|x(k)|^2 + \\ + \cdots]|x(k-q_1)|^2 |x(k-q_2)|^2 x(k)\ , \tag{9}$$

and the successive dynamic components are associated to the corresponding higher-order filtering. Let us emphasize that in this representation the filtering acts directly on the envelope power $|x(k)|^2$, so that the terms of the dynamic component $y_{dr}(k)$ correspond to terms of $(2r)$th-order dynamics in the DDR model [3].

III. DISCUSSION OF THE PRESENT APPROACH

More than a model, here we are presenting a procedure to prune the Volterra-based behavioural model for wideband amplifiers (VBW) [5], referred to as the dynamic VBW approach (DVBW). A first observation about this result is that the coefficients have been regrouped according to the DDR method after a drastic pruning as a consequence of the assumptions outlined in the deduction of the VBW representation. To illustrate the complexity reduction, consider the FV, DDR and DVBW models. For a seventh-order model, with a

memory length of ten delayed samples, and a first-order dynamic reduction (only one-dimensional filtering), the number of coefficients necessary for the FV model is in the order of 105, while the DDR needs 74 coefficients, the MP 44, and the DVBW only 34 coefficients.

In precedent schemes, the structure is commonly truncated to fifth-order terms because of the enormous increase in the complexity and the computational cost of the model. For example, the term $y_5(k)$ of the VBW model involves quadratic filtering, an structure that augments excessively the number of parameters. However, the DVBW proceeds by relocating the term $h_5(0,0)|x(k)|^2x(k)$ in the memoryless part, and the terms associated to one-dimensional filtering into the first-order dynamic characteristic. Likewise, some seventh-order terms of the VBW model are relocated in the memoryless part, and in the first-order and the second-order dynamic characteristics. As in the case of the memoryless part, the first-order dynamic characteristic (8) of a seventh-order DVBW model is more robust to an increase of the input level, because it also includes seventh-order terms. In the structure that emerges, the model order can be large, with a memoryless portion requiring only a few coefficients (four parameters for a seventh-order model), and a trade-off between complexity and precision can be made by controlling the memory length and the dynamic order, analogously to the DDR model [4]. The consequence is a well-suited approach to accurately explain the PA response to excitations in a wide range of levels.

Finally, note that the assumptions of this approach are general and also applicable to wideband PAs with more complicated structures of the thermal filter, or even with other low-frequency dispersive effects, like charge-trapping or impact ionization.

IV. EXPERIMENTAL VALIDATION OF THE APPROACH

In order to test the proposed model, a wideband commercial amplifier has been extensively characterized. The device under test is a medium high PA (model ZHL42W of MiniCircuits Inc., Brooklyn, NY) exhibiting a minimum gain of 30 dB in the frequency range 10–4200 MHz, with a minimum output 1-dB compression point of +28 dBm. The experimental setup has been presented in [10] and is based on an SMIQ02B vector signal generator, from Rohde & Schwarz, Inc., and an E4407B spectrum analyser, from Agilent Technologies Inc., with modulation analysis facility and a bandwidth of the input signal limited to 10 MHz. The PA has been tested utilizing a double set of 2-GHz communication signals with different symbol rates and otherwise modulating parameters in compliance to the UMTS-WCDMA standard. These test signals are referred to as WCDMA-like signals. One set of these digitally modulated signals was used for kernel identification and the other for validation purposes, with 35 different symbol rates in the range from 2 ksym/s to 1 Msym/s, and a power level of –6 dBm, corresponding to the 1-dB input compression point. The peak-to-average ratios (PAPR) for the identification and validation test sets were 4.5 and 4 dB, respectively. For each symbol rate, all the signals were acquired at a sampling rate of 7.5 sa/sym, at least, then were postprocessed from the raw data to correct phase, frequency and timing misalignments, resampled to 5 sa/sym, and the average of 30 acquisitions was calculated. Model

identification was performed by using conventional least squares over 635 aligned samples of the identification signal.

The normalized mean square error (NMSE) of each postprocessed acquisition with respect to the averaged signal was obtained in order to assess the experimental limit of the test bench. Then, the average value of the NMSE obtained among the successive acquisitions of the same probing signal was calculated. By doing this, an estimation of the repeatability of the measured data was obtained, establishing a practical limit for the models accuracy below which their predictions can be considered beyond the experimental uncertainty. According to this, the NMSE results presented in this section have been calculated with the set of validation signals and are expressed with respect to the experimental limit.

The data corresponding to four seventh-order approaches, the memoryless (ML), GMP, DDR and DVBW models, have been represented in Fig. 1 against the symbol rate. In all the structures with memory, a delay of up to $Q = 2$ sa has been assumed, and a first-order dynamic for the DDR and DVBW models has been calculated. With regard to the GMP model, we have used the particular GMP model that provided the best results to the authors of [2]; in particular, the implementation is based on the last row of Table I in the referred paper.

It can be observed that the ML model is adequate for very low symbol rates but departs from the setup limit at low-medium symbol rates. In a band centred in about 20 ksym/s the deviation is distinctly large, indicating the existence of significant low-frequency memory effects [8]. An explanation to this behaviour is that when the symbol rate is very low, the signal bandwidth is large with respect to that of the thermal filter, and the response becomes memoryless. Thus, the resulting model is static. In the other extreme, for signals with a high-enough symbol rate, the time-varying term is significantly attenuated by the thermal low-pass filter, what originates a quasi-static behavior for the PA model (short-term memory). Considering that for some low rates the symbol period is comparable to the memory length of the thermal filter, the contribution of the thermal effects can be significant here (long-term memory). The validation characteristics of the other models show a markedly closeness to the experimental limit in this low-frequency band, an indication that the memory effects are being captured. In particular, the proposed model not only presents a better performance in presence of low-frequency memory effects, but also the highest efficiency, revealed by a significant reduction in the number of coefficients: GMP performs very similarly than DVBW, but at the cost of over the double of coefficients, while DDR exhibits a peak degradation of about 3 dB in this range of symbol rates even with an increase in the number of parameters. Outside this range of rates, and with the exception of a narrow band about 700 ksymb/s, the ML model is not outperformed significantly by the models with memory, in accordance with our previous discussion.

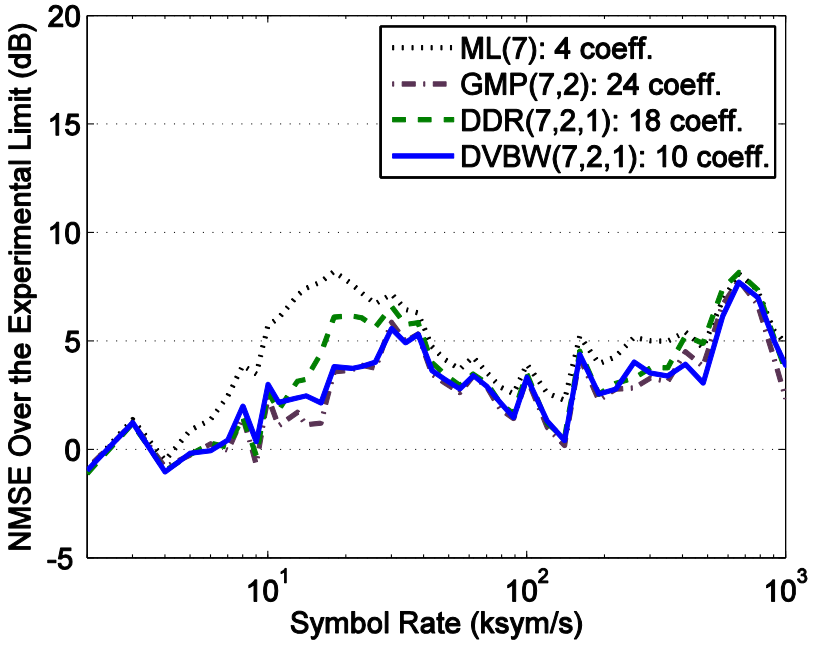

Fig. 1. Comparison of different high-performance seventh-order models representing the response of a commercial PA driven by WCDMA-like signals at different symbol rates, in terms of the improvement of the NMSE over the setup limit.

Although the inclusion of even-order terms in the baseband model has been considered as beneficial in predistortion linearization, a formal deduction of the amplifier model contains only odd-order terms, see (2) of [11]. The positive effect is produced by the richer basis set formed with these even-order terms in a low-order nonlinear model. To investigate the possible favourable effects of these terms, the DDR and GMP models were tested in a range of model delays from $Q = 1$ to $Q = 10$ sa. The implementation of the DDR model with even-order terms is introduced in [12], while that of the GMP model has already been commented. It is important to note that the even-order terms in the baseband model do not come from any even-order term in the bandpass model and the positive effect is significantly reduced as the order of the nonlinear model increases. The best overall results in terms of the NMSE are depicted in Fig. 2 for seventh order, where the models with and without even-order terms are compared for $Q = 2$ sa. It is remarkable that the GMP model does not exhibit a significant improvement by the inclusion of even-order terms, and this trend is followed in the full range of tested model delays. On the other hand, the performance of the DDR model improves when such terms are accounted for in the $Q = 2$ sa case, but it downgrades as the model delay increases, a matter that can be associated to the fact that the vector space spanned by the regressors of the DDR model contains elements that are not representative of the test PA.

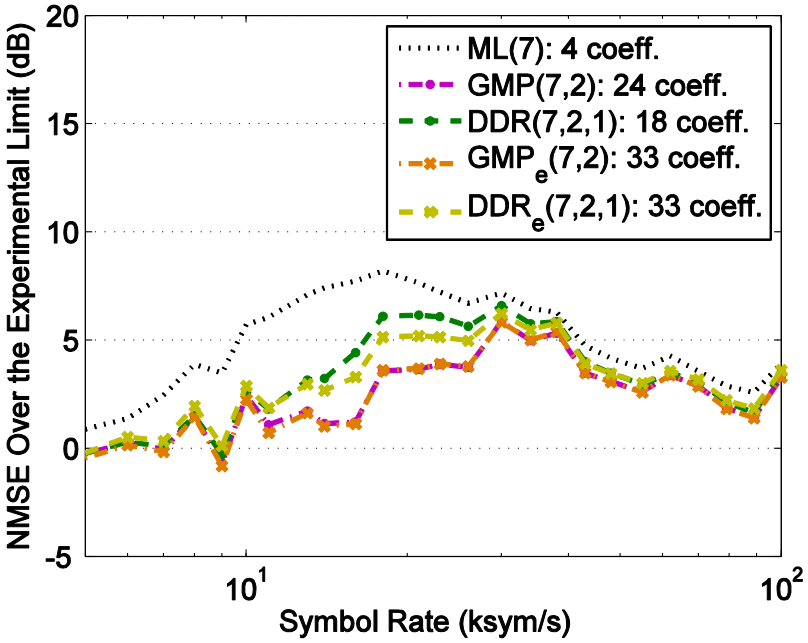

Fig. 2. Comparison of different high-performance seventh-order models with the inclusion of even-order terms: ML (dots), DDR model (dashed lines), and GMP model (dash-dotted lines). The marks correspond to model delays of Q = 2 sa, with odd-order terms only (•), or including even-order terms (×), for WCDMA-like input signals in the ranges of symbol rates from 5 to 100 ksym/s.

We focus now on the DDR and GMP models, with only odd-order terms, together with the DVBW approach, to evaluate their relative performance in the range of symbol rates where the PA exhibits the strongest dynamic effects. The results of Fig. 3 display the departure of the NMSE against the experimental limit for memory lengths of Q = 2 and Q = 10 sa. The DDR model characteristic captures the memory at some rates, but not in all the range, and remains practically invariable with the increase in the number of delayed samples. However, the GMP and DVBW models improve the accuracy considerably, with a deviation over the experimental limit below 5 dB, and their performance is enhanced with the incorporation of more memory. We recall that the GMP model shows the highest structural complexity of the approaches under study, with the largest amount of parameters, and the number of coefficients necessary for the DVBW model approximately halves those of the DDR model. While the selection of memory lengths such as Q = 10 sa may not be an optimal approach for actual applications, this comparison does not change qualitatively for lower values of Q.

According to previous results, a symbol rate of 23 ksym/s was subsequently selected to focus on the frequency band where the PA exhibits a higher deviation from the ML behaviour. The progress of the error as the memory length increases is perfectly observed in Fig. 4, starting with an NMSE = –30 dB, a slight worsening of the error after two delays is clearly observed in the DDR model, what could be an indication of a certain overfitting. On the contrary, the GMP and DVBW models reduce the error monotonically with the incorporation of more delays, reaching an NMSE = –36 dB. Their NMSE improvements compared to DDR can be about 5 dB for Q = 10 sa. At a symbol rate of 1 MHz the NMSE of the ML model is as good

as –40 dB. However, all models show only a slight improvement with the increment of the memory from $Q = 2$ sa, indicating that the low-frequency memory effects are not very significant. As it was mentioned before, observe that the number of coefficients necessary to describe the PA behaviour to meet a target NMSE is not the same for different symbol rates.

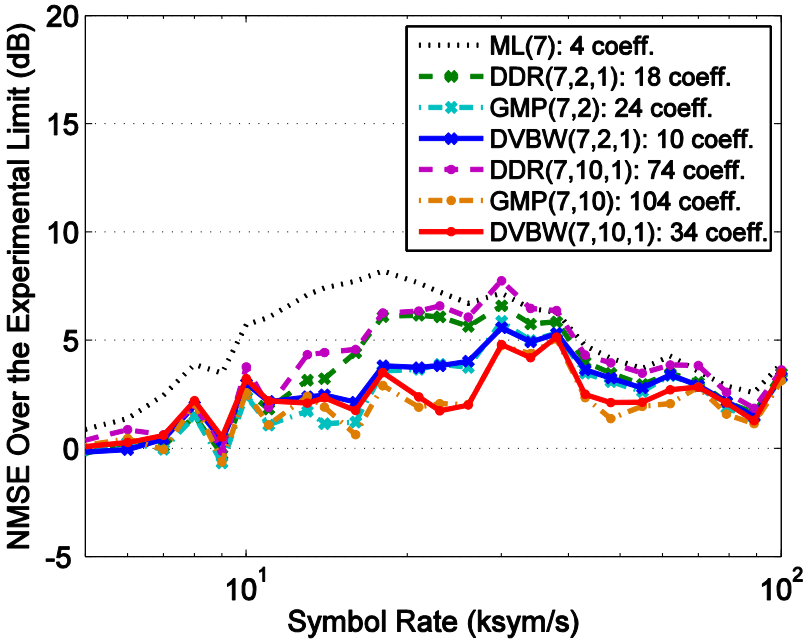

Fig. 3. Performance of seventh-order models in terms of the NMSE: ML (dots), DDR model (dashed lines), GMP model (dash-dotted line) and DVBW model (solid lines). The marks correspond to model delays of $Q = 2$ sa (×) and $Q = 10$ sa (•) for WCDMA-like input signals in the ranges of symbol rates from 5 to 100 ksym/s.

While the prediction of the spectral regrowth is not clearly distinguishable when DDR, GMP and DVBW models are used, the accuracy of the model to represent the spectral regrowth ensures a reliable prediction of the Adjacent Channel Power Ratio (ACPR). The same validation signal waveform was applied to the test PA with input levels swept in the range from –11 dBm to –6 dBm, to measure the left and right ACPR levels, and are represented with marks in Fig. 5. The measured ACPR levels, exhibiting an asymmetry of about 1 dB, were estimated with the DDR and DVBW models from the simulated output waveforms, and are depicted in the same figure. It is remarkable that the left and right ACPR predicted with the DVBW model is closer to the measured values, and the actual difference is within ±1 dB in the full range of levels. These outcomes are also evident in Fig. 6, where the measured spectrum and modelled error spectra are depicted for the highest input level, and a superior performance is obtained with the DVBW model against the DDR model as it is revealed by a lower level for the spectrum of the error signal. Compared to the GMP model, in-band error is very similar, but the proposed model takes the advantage of a significant saving in the number of coefficients (34 versus 104 coefficients for $Q = 10$ sa).

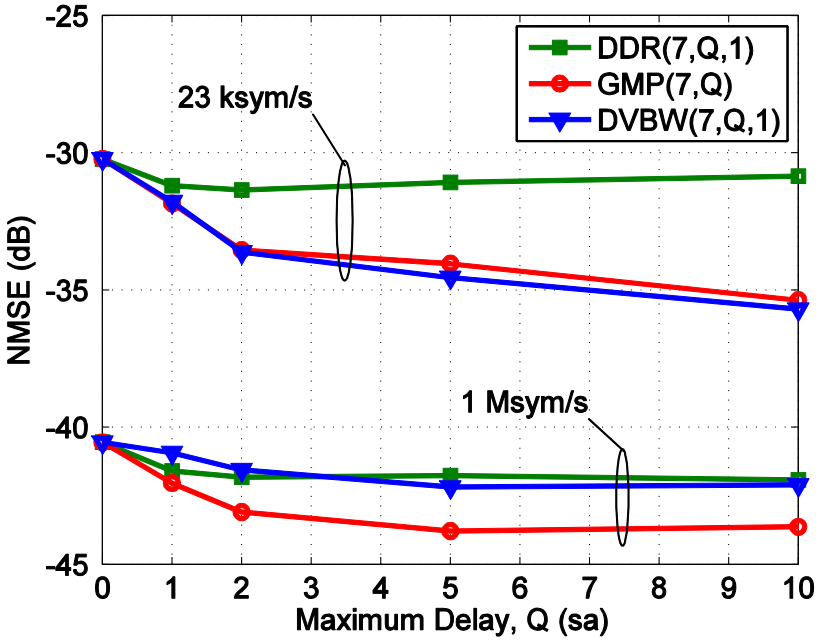

Fig. 4. Validation performance of the seventh-order DDR (□), GMP (○) and DVBW (▽) models in terms of the NMSE as a function of the model delay, for WCDMA-like input signals with symbol rates of 23 ksym/s and 1 Msym/s.

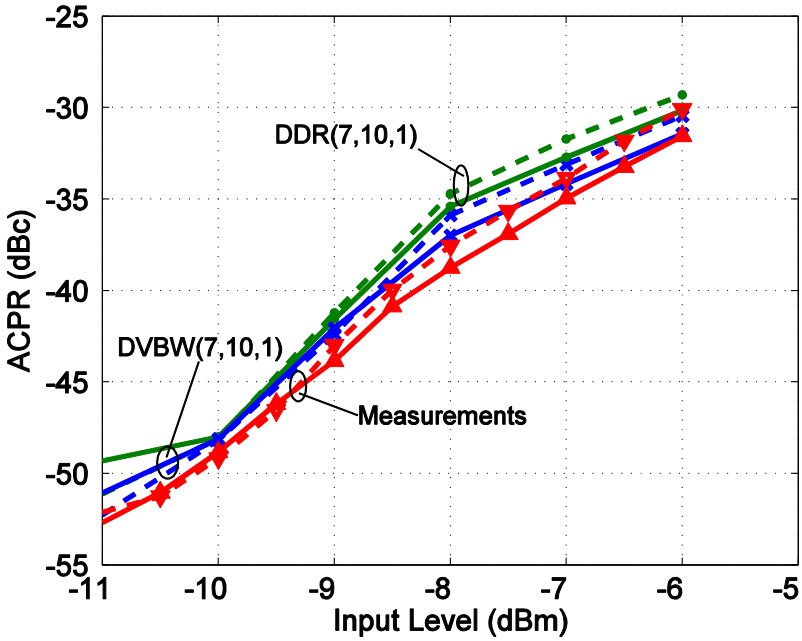

Fig. 5. Measured (△, ▽) and predicted left and right ACPR of a 23-ksym/s WCDMA-like input signal with seventh-order DDR (•) and DVBW (×) models (Q = 10 sa). Dashed-lines correspond to the left ACPR, while solid-lines correspond to the right ACPR.

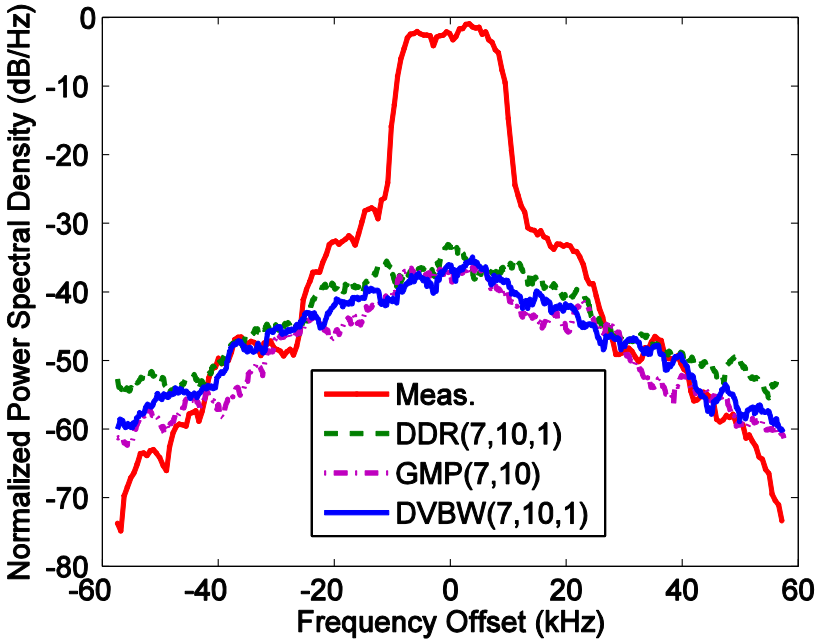

Fig. 6. Measured (marks and solid line) and modelled error spectra (dashed lines) of a 23-ksym/s WCDMA-like input signal with seventh-order DDR, GMP and DVBW models (Q = 10 sa). The error of the spectra is represented in dotted line for the DDR model, in dash-dotted line for the GMP model and in solid line for the DVBW model.

V. CONCLUSION

A new configuration of PA behavioural model has been demonstrated in this paper, which is derived by using a simple equivalent circuit model with thermal effects. The structure can be considered as a particular case of the VBW model, with the kernel coefficients rearranged according to the DDR approach.

We have confronted satisfactorily our results with the previously published high-performance GMP and DDR models. The gain in efficiency of the present approach is evident if it is considered that not only the accuracy is superior, but also that the number of coefficients experiments a radical reduction.

Measurement results on a commercial PA showed the existence of a clear band where the low-frequency dispersive effects are present and where the models have more difficulty to accurately reproduce the experimental data. Comparing the different zones in a symbol rate sweep, we observe that the number of needed coefficients can vary depending on the signal bandwidth.

A future progress of this work is a study of the techniques that can be used in a laboratory context to identify the model parameters. For example, the combined use of pulse measurements to identify the ML parameters, and WCDMA signals to identify the dynamic

part. The implementation of CAD models and algorithms in simulation software and application to linearization of PA are two directions in which this work can be further developed. In particular, the preliminary development of a DVBW-based predistorter for a GaN PA has already been reported by the authors in [13], showing a satisfactory linearization performance compared to other conventional approaches.

ACKNOWLEDGEMENT

This work was completed with the support of the Spanish National Board of Scientific and Technological Research (CICYT) and the Andalusian Government within the projects TEC2011-23559 and P11-TIC-7869.

REFERENCES

[1] Pedro, J.C.; Maas, S.A.: A comparative overview of microwave and wireless power amplifier behavioral approaches. IEEE Trans. Microw. Theory Tech., **53** (2005), 1150–1163.

[2] Morgan, D.R.; Ma, Z.; Kim, J.; Zierdt, M.G.; Pastalan, J.: A generalized memory polynomial model for digital predistortion of RF power amplifiers. IEEE Trans. Signal Process., **54** (2006), 3852–3860.

[3] Zhu, A.; Dooley, J.; Brazil, T.J.: Simplified Volterra series based behavioral modeling of RF power amplifiers using deviation-reduction, IEEE MTT-S Int. Microwave Symp. Dig., San Francisco, CA, 2006.

[4] Zhu, A.; Pedro, J.C.; Brazil, T.J.: Dynamic deviation reduction-based Volterra behavioral modeling of RF power amplifiers. IEEE Trans. Microw. Theory Tech., **54** (2006), 4323–4332.

[5] Crespo-Cadenas, C.; Reina-Tosina, J.; Madero-Ayora, M.J.: Volterra behavioral model for wideband RF amplifiers. IEEE Trans. Microw. Theory Tech., **55** (2007), 449–457.

[6] Cunha, T.R.; Pedro, J.C.; Cabral, P.M.: Design of a power-amplifier feed-forward RF model with physical knowledge considerations. IEEE Trans. Microw. Theory Tech., **55** (2007), 2747–2756.

[7] Crespo-Cadenas, C.; Reina-Tosina, J.; Madero-Ayora, M.J.: An equivalent circuit-based approach to behavioral modeling of long-term memory effects in wideband amplifiers. Microw. Opt. Technol. Lett., **53** (2011), 2278–2281.

[8] Crespo-Cadenas, C.; Reina-Tosina, J.; Madero-Ayora, M.J.: Study of a power amplifier behavioral model with nonlinear thermal effects, Proc. 40th European Microw. Conf., Paris, France (2010).

[9] Minasian, R.A.: Intermodulation distortion analysis of MESFET amplifiers using the Volterra series representation. IEEE Trans. Microw. Theory Tech., **28** (1980), 1–8.

[10] Reina-Tosina, J.; Crespo-Cadenas, C.; Madero-Ayora, M.J.: A compact Volterra model for power amplifiers with memory, IEEE MTT-S Int. Microwave Symp. Dig., Boston, MA (2009).

[11] Ding, L.; Zhou, G.T.: Effects of even-order nonlinear terms on power amplifier modeling and predistortion linearization. IEEE Trans. Vehicular Technol., **53** (2004), 156–162.

[12] Lima, E.G.; Cunha, T.R.; Pirola, M.; Pedro, J.C.: Baseband derived Volterra series for power amplifier modeling, IEEE MTT-S Int. Microwave Symp. Dig., Boston, MA (2009).

[13] Madero-Ayora, M.J.; Dine, M.S.E.; Neveux, G.; Nebus, J.M.; Reina-Tosina, J.; Allegue-Martinez, M.; Crespo-Cadenas, C.: Baseband digital predistortion of a 10 W GaN power amplifier, Proc. 41st European Microw. Conf., Manchester, UK (2011).

Bibliographies

Carlos Crespo-Cadenas was born in Madrid, Spain. He received the degree in Physics in 1973 and Doctor degree in 1995 from the Polytechnique University of Madrid. Since 1998 he has been Associate Professor and currently he teaches lectures on Radio Communications in the Department of Signal Theory and Communications, University of Seville. His current interests are Nonlinear Analysis applied to Wireless Digital Communications and to Microwave Monolithic Integrated Circuits (MMIC).

Javier Reina-Tosina was born in Seville, Spain. He received the Telecommunication Engineering and Doctor degrees from the University of Seville, Seville, Spain, in 1996 and 2003, respectively. Since 1997 he has been with the Department of Signal Theory and Communications, University of Seville, where he is currently an Associate Professor. His research interests include MMIC technology, nonlinear analysis of active microwave devices and integration of information technologies in biomedicine.

María J. Madero-Ayora received the Telecommunication Engineering and Doctor degrees from the University of Seville, Seville, Spain, in 2002 and 2008, respectively. Since 2003 she has been with the Department of Signal Theory and Communications, University of Seville, and is currently Associate Professor. Her research interests focus on the

area of nonlinear analysis of active microwave devices and measurement techniques for nonlinear communication systems.

List of figures